Australasian Physical & Engineering Sciences in Medicine (2019) 42:211–220
https://doi.org/10.1007/s13246-019-00732-x

SCIENTIFIC PAPER

The effect of fluorescence on surface dose with superficial X-rays incident on tissue with underlying lead

John Baines[1] · S. Zawlodzka[1] · T. Markwell[1] · M. Chan[1]

Received: 12 September 2018 / Accepted: 29 January 2019 / Published online: 6 February 2019
© Australasian College of Physical Scientists and Engineers in Medicine 2019

Abstract

An Advanced Markus chamber on the surface of solid water phantom was used to determine surface dose reduction, with either a lead or air interface, as a function of surface-interface separation (t). The beam quality dependence of dose reduction was investigated using the 50 kV, 100 kV and 150 kV beams of an Xstrahl 150 superficial X-ray unit. For each beam the dose correction factor, DCF(t), namely the ratio of surface dose (t) to surface dose (t = 100 mm), was determined. Monte Carlo simulations of DCF(t) with a lead interface were compared with corresponding measured values. Simulated spectra were calculated at the phantom surface for full backscatter (t = 100 mm) and with either a lead or air interface at 2 mm or 8 mm depth. For each depth and beam quality lead fluorescent radiation at the surface was evident. The variation of DCF(t) for each beam and field size exhibits a minima at $t \approx 5$ mm and in the range 1 mm $\leq t \leq$ 40 mm surface dose reduction is larger for 100 kV than 150 kV. Monte Carlo simulated DCF(t) are consistent with corresponding measured DCF(t). From simulated spectra L-series fluorescent X-rays ($\approx$ 15 keV) emanating from lead at t = 2 mm are evident for all beams and fluorescent K-series X-rays only occur with 100 kV and 150 kV beams.

Keywords Superficial X-rays · Backscatter reduction due to lead

Introduction

The use of kilovoltage X-rays in the treatment of superficial lesions is advantageous due to the fact that maximum dose deposition occurs at the skin surface. To protect tissue surrounding a lesion lead shielding is commonly used. In certain situations, shielding is placed under tissue and downstream of the beam, as in treatments of the pinna. In such cases surface dose is reduced due to the lack of tissue and resulting loss of backscatter radiation [1]. Loss of backscatter due to the presence of underlying lead in tissue has been investigated and it is known that for a given beam energy surface dose is reduced as the surface-lead separation decreases. Further as beam quality increases from 1 mm to 8 mm Al HVL loss of surface dose increases for a given separation [2]. For such beam qualities the departure from full backscatter conditions incurred with a lead interface is associated with the energy dependent loss of tissue Compton backscatter [3–5]. Comparing lead backscatter effects for the 5 mm Al HVL and 13 mm Al HVL beams of a Pantak SXT 150 unit Healy et al. [6] observed smaller surface dose reduction effects at the higher beam quality. Monte Carlo backscatter simulations and measured data for beams generated by a Pantak DXT 300 unit demonstrated similar surface dose behaviour for 4 mm Al HVL and 7.2 mm Al HVL beams [5]. Further in the recent commissioning of an Xstrahl 150 unit at our institution, and reported in this work, surface dose reduction for a given surface-lead separation < 40 mm is less at 150 kV (8.5 mm Al HVL) than 100 kV (3 mm Al HVL). The combined effects of loss of Compton backscatter due to the absence of tissue, associated with the presence of lead, and the generation of fluorescent photons by lead has been suggested for this energy dependent surface dose reduction. Depending on incident energy, fluorescent photons are generated by lead that can contribute to the surface dose and therefore counteract the effects of loss of Compton backscatter due to absence of tissue [5, 7].

Many investigations of surface dose reduction with underlying lead were limited to a minimum surface-lead separation of 5 mm [2, 5, 6, 8]. In the work of Healy et al. [6] there was an indication that at 5 mm the dose reduction was less

✉ John Baines
john.baines@health.qld.gov.au

[1] Radiation Oncology Princess Alexandra Hospital, 31 Raymond Terrace, Brisbane, QLD 4101, Australia

than at 7 mm for beam qualities 1 mm Al HVL and 13 mm Al HVL. On the contrary such behaviour was not evident in other complementary studies of backscatter reduction due to underlying lead [3, 5]. To further investigate surface dose reduction with underlying lead for $t \leq 5$ mm these authors used an Advanced Markus chamber with its entrance window facing downstream on the surface of a solid water phantom. The use of parallel plate chambers in such an orientation to measure backscatter reduction effects has been reported previously [3, 9]. With this chamber orientation it is possible to use the Advanced Markus chamber to investigate surface dose reduction with a surface-lead separation t between 1 and 100 mm [10]. By comparison with corresponding air interface measurements, a perfect absorber, the effect of lead fluorescence on surface dose can be demonstrated for this range of tissue thickness.

In this work an Advanced Markus chamber with entrance window facing downstream was used to investigate surface dose reduction with surface-lead and surface-air separation t between 1 mm and 100 mm. This extends the work of Healy et al. [6] that determined surface dose reduction with underlying lead for $t \geq 5$ mm using a Farmer (NE2577) chamber (0.2 cm^3).

Furthermore, Monte Carlo simulations were used to calculate surface dose reduction with underlying lead for t = 1–100 mm and comparison with measured surface dose reduction is presented. Monte Carlo simulated spectra at the surface of a water phantom with underlying air or lead provide a means to correlate missing tissue backscatter and lead fluorescence with measured surface dose reduction as a function of beam quality.

Materials and methods

Chamber measurements

X-ray beam qualities (Q) of 1 mm Al HVL (50 kV), 3 mm Al HVL (100 kV) and 8.5 mm Al HVL (150 kV) generated by an Xstrahl 150 therapy system were used in this investigation. Circular fields of diameter (ϕ) 2.5 cm and 5 cm were normally incident on the surface of a solid water phantom the water equivalence of which for superficial energies has been previously reported [11]. In order to facilitate surface dose measurements for t = [1–3, 5, 8, 10, 15, 20, 30, 40, 60, 80, 100] mm an Advanced Markus chamber (PTW, Freiburg, Germany Type 34045) was centrally located within each beam with the active volume adjacent to the solid water surface (Fig. 1). By way of comparison a Farmer type thimble chamber NE2577 (0.2 cm^3) was also used to measure DCF(t) with underlying lead for t = 5, 10, 20 and 40 mm. For these measurements the chamber was recessed within a solid water slab such that the central electrode was aligned with the surface [10]. Within the slab the distance from the central electrode to the base of the slab is 5 mm and as such sets a lower limit (t = 5 mm) on the distance to the lead interface. A UNIDOS^{webline} electrometer (PTW, Freiburg, Germany) was used with each chamber and readings were obtained for each surface-interface separation and DCF (t, applicator, interface, Q) calculated using Eq. 1,

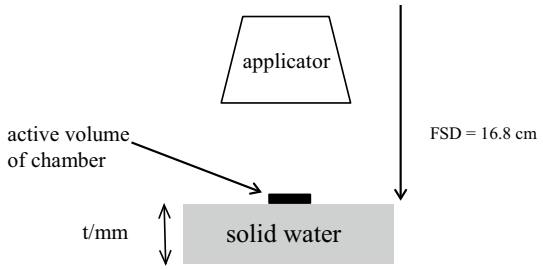

Fig. 1 Schematic diagram (not to scale) of the Advanced Markus active volume adjacent to phantom surface. Lead and air interfaces are at a depth t/mm below the phantom surface. Applicator 18 mm above surface

$$DCF(t,\ applicator,\ interface,\ Q) = \frac{M(t,\ applicator,\ interface,\ Q)}{M_{100}(applicator,\ Q)}, \quad (1)$$

where M is chamber measurement for surface-interface separation t and M_{100} is the chamber measurement with 100 mm solid water (full backscatter).

For all chamber measurements the applicator to solid water surface separation was 18 mm in order that the Advanced Markus chamber (height 14 mm) can be reproducibly positioned between the surface and the applicator.

Monte Carlo simulations

Simulations of Xstrahl 150 beams incident on water with lead or air interfaces at various depths t/mm from the water surface were derived using Electron Gamma Shower (EGSnrc) v4-r2-4-0 [12–14] and a model of the Xstrahl 150 unit, X ray interactions and calculation options as described previously [10].

Using DOSXYZnrc [15] simulated surface doses were obtained by averaging the calculated dose within four $2.5 \times 2.5 \times 1$ mm^3 voxels around the beam central axis (CAX) at the phantom surface (Fig. 2) for full backscatter (t = 100 mm) and with surface-lead separations, t, between 1 and 100 mm. Simulated DCF(t) were derived from the ratio of surface dose with separation (t) to surface dose with full backscatter (t = 100 mm). To investigate DCF(t) in the absence of lead L-series fluorescent X-rays (≈ 15 keV) simulated surface doses for 100 kV were derived using PCUT = 0.02 MeV. For all Monte

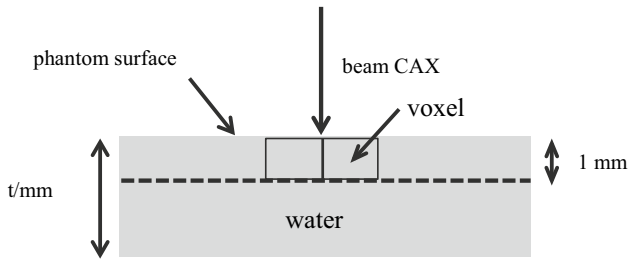

Fig. 2 Schematic diagram (not to scale) showing 2 of 4 DOSXYZnrc calculation voxels distributed about the CAX, within a superficial segment of depth 1 mm

Carlo based DCF(t) values uncertainties were estimated from errors listed in DOSXYZnrc files and were < 0.5% (1 SD).

Spectra with full backscatter conditions and with a lead or air interface at 2 mm or 8 mm depth from the surface, $\phi = 5$ cm, were calculated from phase space files using 1×10^7 histories and analysed using BEAMDP [16]. The calculation volume consisted of a cylinder of diameter 5 mm and depth 1 mm located within a 1 mm layer below the surface. A further 1 mm or 7 mm water slab was included to achieve the interface depths referred to above. For spectral simulations the photon cross-section option XCOM was selected which is suitable in the context of this investigation [17, 18] and estimated intensity uncertainties were ≈ 0.5% (1SD).

For a given energy the difference between the full backscatter spectrum at the surface and the spectrum calculated with an 8 mm surface-air separation generates the missing backscatter spectral distribution due to air at this depth. The difference between the calculated surface spectrum with a lead interface at depth t mm and an air interface at the same depth was determined for t = 2 mm and 8 mm. These difference spectra represent the fluorescent and non-fluorescent surface spectral components produced by lead at both depths.

Results

Comparison of DCF(t) obtained with the Farmer and Advanced Markus chambers

Table 1 shows DCF(t, lead) values obtained using the NE2577 Farmer chamber and differences (DCF^{farmer} – $DCF^{advanced\ Markus}$) between corresponding farmer and advanced Markus based values. For a separation 10 mm ≤ t ≤ 40 mm the range of differences 0.012 to − 0.008 is comparable to previously reported chamber inter-comparisons with air and bone interfaces [10]. In the vicinity of the minima DCF(t = 5 mm, lead, Q) chamber differences increase with decreasing beam quality with a maximum difference of 0.021 for 50 kV.

Surface dose reduction due to lead and air interfaces

For both field sizes (Figs. 3, 4) the variation of measured DCF(t, lead, Q) for t > 5 mm is consistent with that observed by other investigators for beams of comparable quality and field size [5, 6]. The presence of a minima at t ≈ 5 mm is evident, independent of beam quality and field size. The 100 kV beam shows the largest decrease in DCF as t approaches 5 mm with values at the minima for the 5 cm (2.5 cm) applicator of 0.91 (0.96) compared to 0.94 (0.98) and 0.96 (0.98) for 150 kV and 50 kV, respectively. For t < 5 mm, DCF(t, lead) for each applicator and energy increases and at t = 1 mm, $\phi = 2.5$ cm, DCF(t, lead) is greater than unity for all beams. In the region t ≤ 20 mm DCF(t, air) is significantly less than DCF(t, lead) for the 150 kV beam, $\phi = 5$ cm (Fig. 3c). In contrast, for 50 kV and 100 kV beams significant differences between DCF(t, air, Q) and DCF(t, lead, Q) appear for t < 8 mm. At t = 8 mm, $\phi = 5$ cm, DCF(t, air) is 0.92 and 0.91 for 100 kV and 150 kV, respectively. In contrast corresponding values at the same depth for DCF(t, lead) are 0.93 and 0.95. For $\phi = 2.5$ cm beams, t = 8 mm, DCF(t, air) ≈ 0.96 for 100 kV and 150 kV whilst DCF(t = 8 mm, lead) is 0.97 and 0.98 for 100 kV and 150 kV, respectively (Fig. 4). For both field sizes the introduction of lead

Table 1 Lead interface DCF(t) values for 2.5 cm and 5 cm diameter field sizes measured with the NE2577C farmer chamber and differences (DCF^{farmer} – $DCF^{advanced\ Markus}$) in brackets ()

Energy (kV)	Field	Measurement derived DCF(t) with a lead interface			
		t = 5 mm	t = 10 mm	t = 20 mm	t = 40 mm
50	$\phi = 2.5$	0.999 (0.021)	0.988 (0.003)	0.997 (0.004)	0.999 (0.003)
	$\phi = 5.0$	0.979 (0.021)	0.981 (0.012)	0.996 (0.008)	1.004 (0.008)
100	$\phi = 2.5$	0.979 (0.015)	0.976 (0.002)	0.993 (0.005)	0.999 (0.003)
	$\phi = 5.0$	0.932 (0.017)	0.942 (0.002)	0.972 (0.003)	0.995 (0.006)
150	$\phi = 2.5$	0.992 (0.007)	0.983 (− 0.001)	0.994 (0.005)	1.000 (0.006)
	$\phi = 5.0$	0.934 (− 0.004)	0.943 (− 0.008)	0.966 (− 0.006)	0.989 (− 0.004)

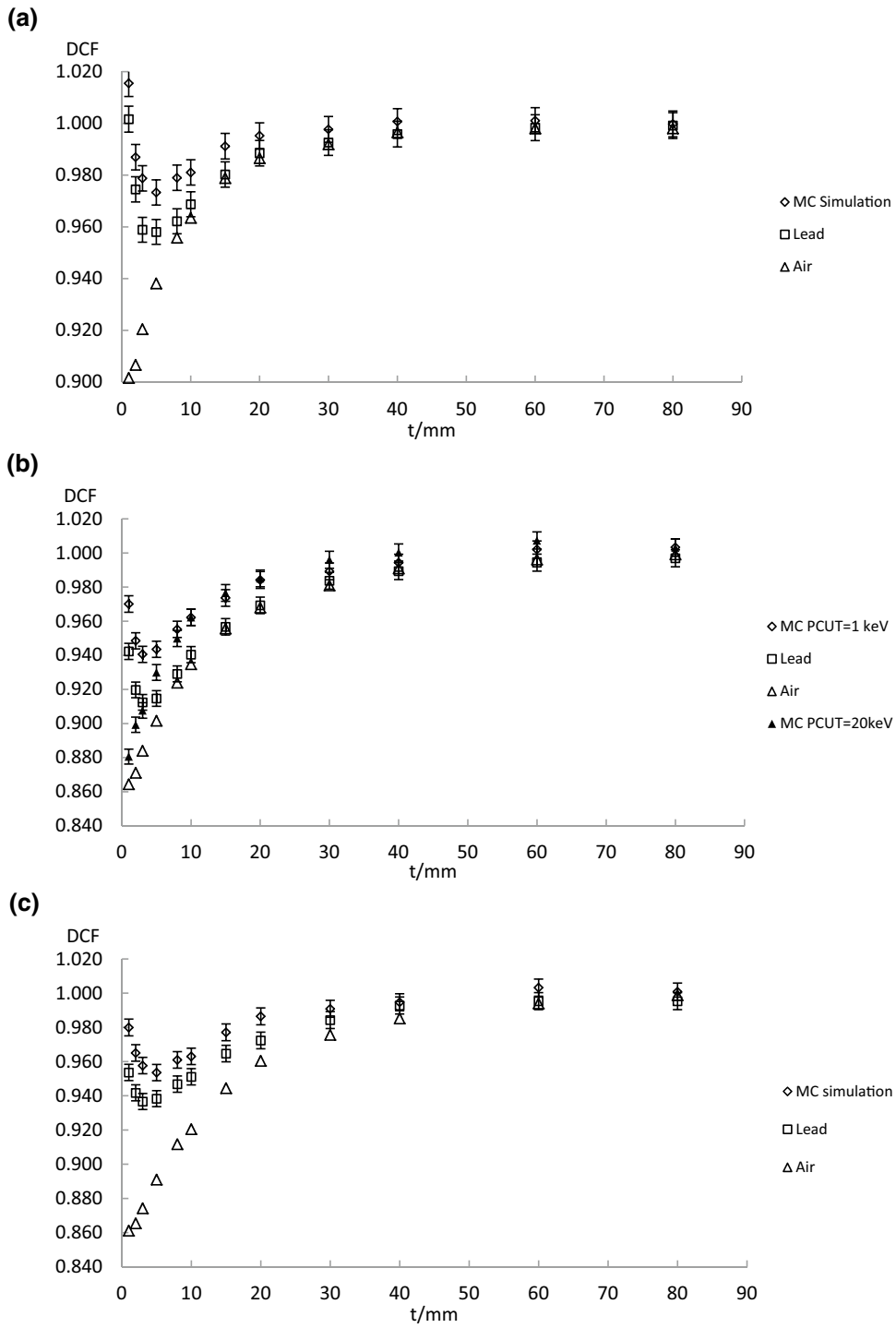

Fig. 3 Simulated and measured dose correction factor (DCF) as a function of surface-lead/air interface separation (t) for **a** 50 kV, **b** 100 kV and **c** 150 kV, ϕ = 5 cm. As DCF (t = 80 mm) = 1 presented data limited to t = 80 mm. Error bars (± 0.5%) omitted from air data

increases DCF(t = 8 mm, Q) relative to the air interface value and this effect is greatest for the 150 kV, ϕ = 5 cm, beam.

Monte Carlo modelling of surface dose reduction

Qualitatively the variation of measured and simulated DCF(t) are in agreement with each exhibiting a minima in the region of t ≈ 5 mm (Figs. 3, 4). Maximum differences of 1.5% and 3% are observed for 100 kV and occur at the minima for the 2.5 cm and 5 cm applicator, respectively. With PCUT = 20 keV simulated DCF(t) for 100 kV does not have a minima and for t ≥ 8 mm approaches the variation of DCF(t) calculated with PCUT = 1 keV (Fig. 3). The relative variation of DCF(t > 5 mm) for 50 kV, 100 kV and 150 kV is in accord with that reported for simulated beams of comparable quality [5].

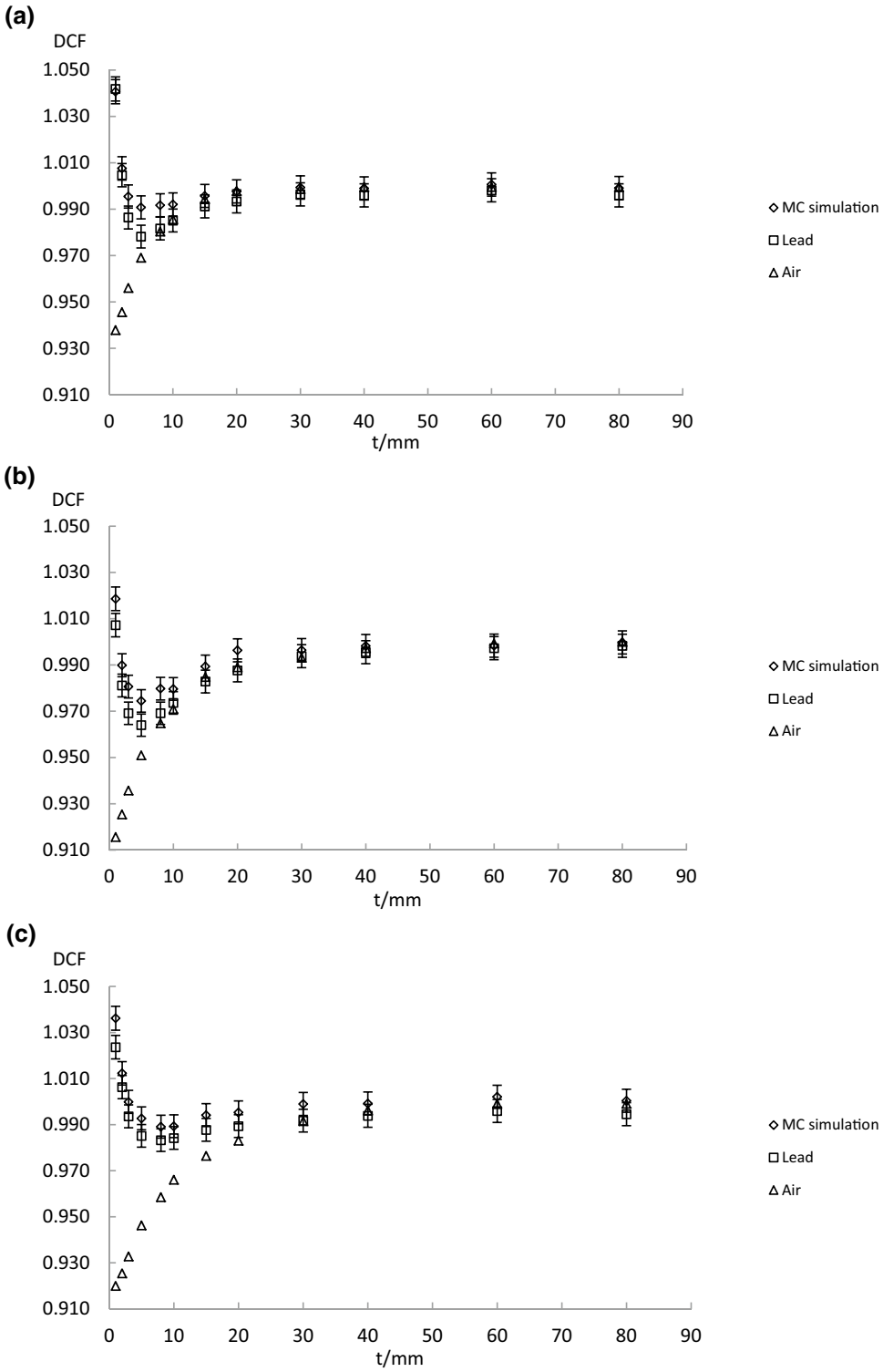

Fig. 4 Simulated and measured dose correction factor (DCF) as a function of surface-lead/air interface separation (t) for **a** 50 kV, **b** 100 kV and **c** 150 kV, $\phi = 2.5$ cm. As DCF (t = 80 mm) = 1 presented data limited to t = 80 mm. Error bars (±0.5%) omitted from air data

Monte Carlo simulated spectra

Figure 5 shows the 150 kV photon spectrum at the tissue surface calculated with a lead interface at 8 mm depth. Characteristic $K_\alpha(W) \approx 59$ keV and $K_\beta(W) \approx 67$ keV lines due to the Xstrahl tungsten target are present and at ≈48 keV there is a perturbation of the continuous background that is consistent with the Compton backscatter of $K_\alpha(W)$ radiation and evident in previous work [19]. Additionally, characteristic lead $K_\alpha(Pb) \approx 75$ keV and $K_\beta(Pb) \approx 85$ keV lines are evident.

Spectra at the water surface produced exclusively by lead at either 2 mm or 8 mm depth shows the presence of

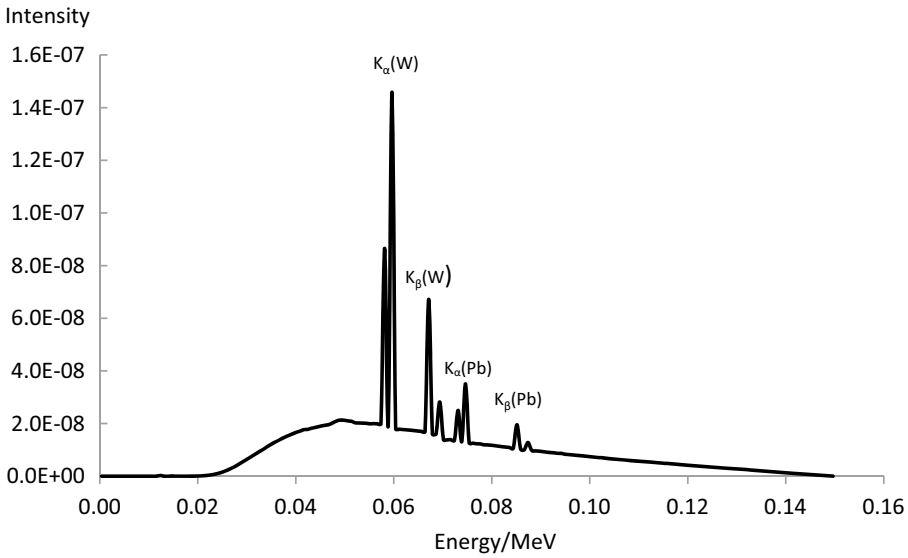

Fig. 5 150 kV spectrum at the tissue surface with a lead interface at 8 mm depth, $\phi = 5$ cm

fluorescence with L-series X-rays (≈ 15 keV) for all beams whilst K-series X-rays only occur for the 100 kV and 150 kV beams (Fig. 6). The appearance of K-series X-rays contrasts with the observations of Hill et al. [5] based on Monte Carlo simulations of lead backscatter with the 75 kV and 100 kV beams of a Pantak DXT 300 X-ray unit.

The intensity of L-series X-rays decreases with increasing depth and beam energy (Fig. 6). The surface spectrum intensity ratio K_α(75 keV):L-series(≈ 15 keV) with lead at 8 mm is approximately 7:1 and 77:1 for 100 kV and 150 kV, respectively. Further at the same depth the intensity ratio of K_α (75 keV) at 150 kV and 100 kV is approximately 10:1. For all kV beams it is observed that non-fluorescent spectral components at the surface, such as Compton backscatter from lead, are not present to a significant extent (Fig. 6).

Figure 7 shows a comparison of Compton backscatter spectral losses from tissue and K-series X-rays at the surface with lead present at 8 mm depth for 100 kV and 150 kV. For 150 kV the proportion of fluorescent X-rays to missing backscatter is greater than that at 100 kV. The peak at ≈ 48 keV in the missing backscatter spectra is associated with tissue Compton backscatter of tungsten K_α(≈ 59 keV) X-rays. For 150 kV at 53 keV there is also evidence for the Compton backscatter of tungsten $K_\beta \approx 67$ keV X-rays.

Discussion

Comparison of DCF(t) values measured with a Farmer (NE2577) and Advanced Markus chamber as described in this work has been previously reported for air and bone interfaces [10]. With a lead interface the maximum difference ($DCF^{farmer} - DCF^{advanced\ Markus}$) is 0.021 and occurs at $t = 5$ mm for the 50 kV beam (Table 1). For all beams it has been shown that L-series X-rays are incident on the surface and for $t = 2$ mm the relative intensity is greatest at 50 kV (Fig. 6). For this energy Farmer chamber readings would tend to be higher than the Markus chamber given that for $t = 5$ mm there is ≈ 2 mm of solid water between the lead and Farmer chamber cavity on the beam central axis [6]. Reduced L-series fluorescence at 150 kV relative to 100 kV is also consistent with a smaller difference ($DCF^{farmer} - DCF^{advanced\ Markus}$) at $t = 5$ mm for the higher energy beam. With $t \geq 10$ mm chamber differences decrease for all beams as would be expected given the average range ≈ 6 mm of L-series X-rays in water ($\mu/\rho = 1.673$ cm^2/g) [20]. Overall the chamber comparison does not suggest that the use of the Advanced Markus chamber with entrance window downstream is problematic in the context of this investigation.

Differences ($DCF^{farmer} - DCF^{advanced\ Markus}$) could be associated with the relative response of each chamber at low energies and this requires further investigation outside the scope of this work.

The qualitative agreement between measured and Monte Carlo DCF(t) variations with beam quality and field size further supports the use of the Advanced Markus chamber as described. Monte Carlo simulations incorporating a model of the Advanced Markus chamber would be recommended for future work.

For both field sizes and all beam energies investigated it has been shown that the variation of measured and simulated DCF(t) with depth (t) to underlying lead exhibit a minima at $t \approx 5$ mm. The observation of such a minima has not been previously reported with chamber based measurements. However in the EBT2 film investigation of Eaton et al. [21] similar behaviour is evident for the 60 kV (1 mm Al HVL) and 120 kV (5 mm Al HVL) beams of a Gulmay D3225 unit.

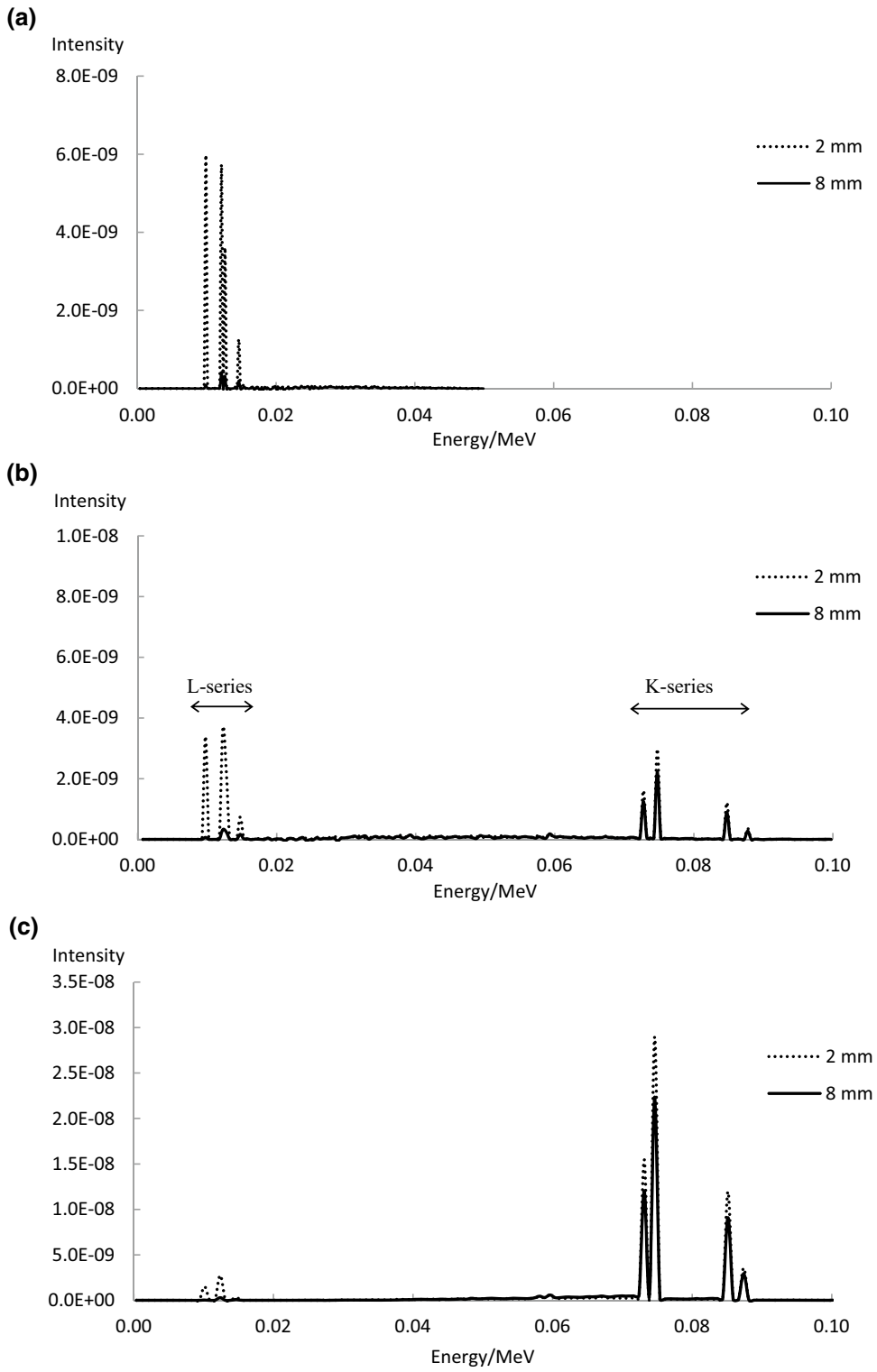

Fig. 6 Lead L-series and K-series X-rays with surface-interface separations of 2 mm and 8 mm for **a** 50 kV and **b** 100 kV and **c** 150 kV (truncated scale), $\phi = 5$ cm

Observed differences between measured and Monte Carlo DCF(t) values can be attributed in part to chamber perturbations that appear to have a greater influence for the larger applicator. For this applicator radiation emanating from the field edges at the lead interface has a greater effective path length through the body of the chamber as t decreases. Increased attenuation particularly for L-series X-rays would tend to decrease measured DCF(t). Such an effect would occur to a lesser extent for $\phi = 2.5$ cm given that the chamber-applicator geometry reduces the obliquity

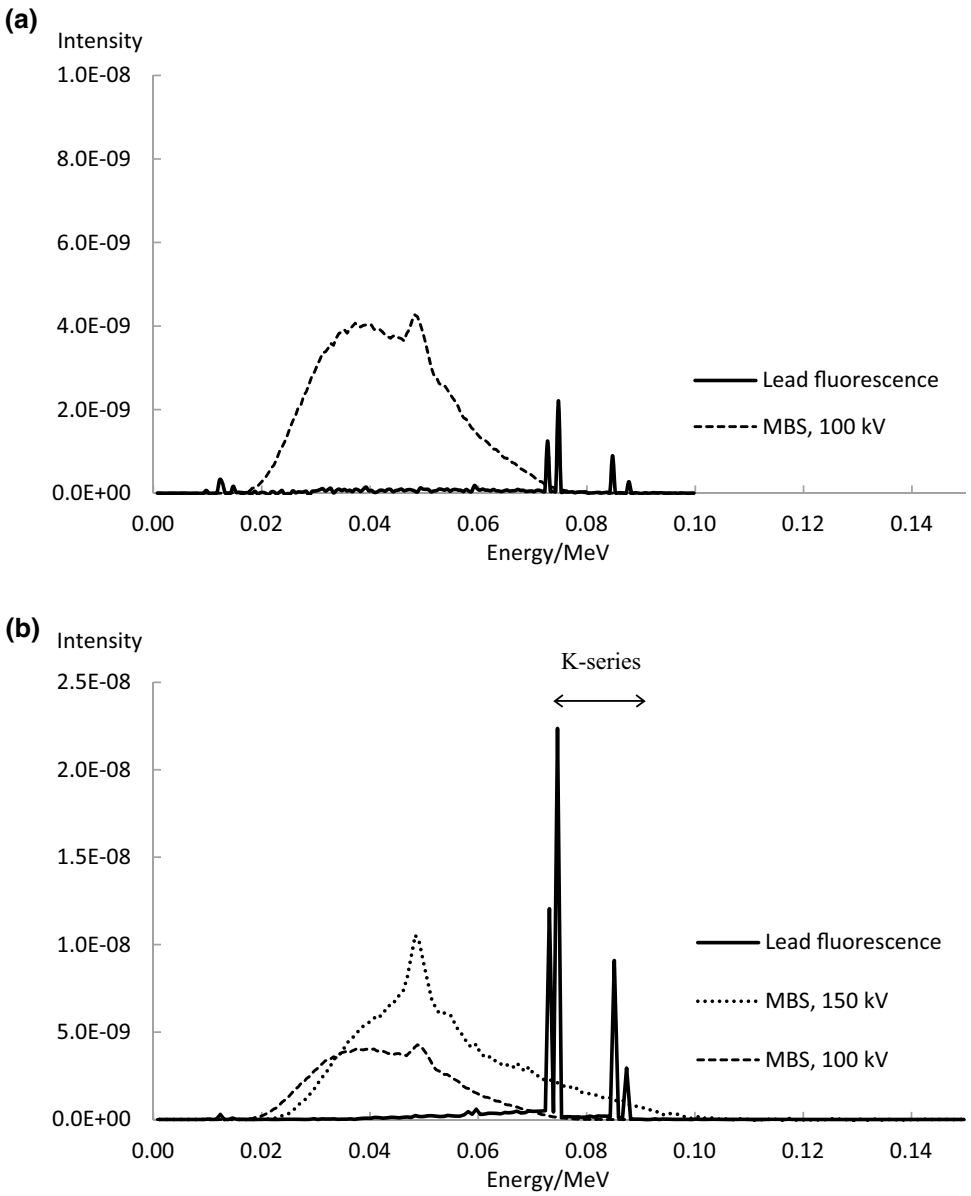

Fig. 7 Fluorescent X-rays associated with lead at 8 mm and missing backscatter spectra (MBS) at the surface with 8 mm tissue (no lead) for **a** 100 kV and **b** 150 kV (100 kV missing backscatter spectra included for comparison), $\phi = 5$ cm

of backscatter radiation directed towards the active volume of the chamber.

At the phantom surface spectra associated with underlying lead at 2 mm or 8 mm consist predominantly of lead K and L fluorescent X-rays. The average range of L-series X-rays in water ≈ 6 mm is consistent with the greater intensity of these X-rays for a given primary beam with lead at 2 mm depth (Fig. 6). L-series X-rays are the only source of lead fluorescence at 50 kV and it is observed that with $t \geq 8$ mm DCF(t, applicator, air) $\approx$ DCF(t, applicator, lead) for this beam (Figs. 3, 4). For such depths surface dose reduction due to air and lead interfaces are comparable, in effect lead fluorescence has a negligible impact on surface dose. However for $t \leq 5$ mm DCF(t, applicator, lead) > DCF(t, applicator, air) and the source of this difference may be explained by L-series X-rays partially offsetting the loss of tissue backscatter with lead at these depths. Given that L-series X-rays are common to all beams investigated suggests that such X-rays contribute to the appearance of a minima in the variation of DCF(t, applicator, lead, Q) at $t \approx 5$ mm. Indeed it has been demonstrated that for 100 kV, $\phi = 5$ cm, simulated DCF(t) with PCUT = 20 keV does not exhibit a minima and at $t = 8$ mm approaches DCF(t) calculated with PCUT = 1 keV (Fig. 3b).

It has been reported that with underlying lead in tissue 100 kV beams exhibit a greater surface dose reduction with decreasing tissue thickness than beams of higher quality [5, 6]. Such observations are in accord with the behaviour reported in this work (Figs. 3, 4). Comparing the loss of Compton backscatter ($t = 8$ mm) for 100 kV and 150 kV it is

evident that greater loss occurs at the higher energy (Fig. 7). However the primary beam fluence for 150 kV is greater than that for 100 kV and it is observed that DCF(t = 8 mm, air) is 0.92 and 0.91 for 100 kV and 150 kV, respectively. This implies that at this depth the impact of missing backscatter on surface dose is approximately equivalent for these beams although the loss of backscatter is different for each beam. In conjunction with fluorescence due to underlying lead corresponding DCF(t = 8 mm) values are 0.93 and 0.95 for 100 kV and 150 kV, respectively. In the presence of lead the greater increase of DCF(t = 8 mm, lead) relative to DCF(t = 8 mm, air) for 150 kV is suggested by the relative K-series yield for this energy compared to 100 kV (Fig. 7). For 8 mm ≤ t ≤ 40 mm DCF(t, 100 kV) for lead and air interfaces are comparable which implies that the influence of lead K-series fluorescence on surface dose is negligible (Figs. 3, 4). This is in agreement with the spectral analysis of Hill et al. [5]. In contrast within the same range of tissue thickness differences between DCF(t, applicator, lead, 150 kV) and DCF(t, applicator, air, 150 kV) are clearly evident (Figs. 3, 4). As the average range of K_α X-rays in water is approximately 50 mm ($\mu/\rho = 1.837 \times 10^{-1}$ cm^2/g) [20] it is feasible for K-series fluorescence at 150 kV to contribute to surface dose for t < 40 mm. Hence it would be expected that in this range of tissue thickness DCF(150 kV) > DCF(100 kV). Although K-series X-rays offset the loss of tissue backscatter to varying extents for 100 kV and 150 kV the additional source of L-series X-rays at the surface for t < 6 mm appears to contribute to the observed minima in the variation of DCF(t) for all beams investigated.

Conclusion

Using an Advanced Markus chamber with entrance window facing downstream on the surface of a phantom lead backscatter reduction effects on surface dose have been investigated down to surface-lead separations of 1 mm. With this chamber arrangement the appearance of a minima in the variation of DCF(t) at t ≈ 5 mm has been observed for all energies. The appearance of a minima is also a feature of the Monte Carlo simulated variation of DCF(t, applicator, lead, Q) and has not been previously reported. Monte Carlo calculated surface spectra suggest that the increase in DCF(t, applicator, lead, Q) for t < 6 mm is associated with L-series X-rays emanating from lead. For t < 40 mm lead K-series X-rays significantly influence surface dose for 150 kV in contrast to 50 kV and 100 kV. The significance of L-series X-rays for t < 6 mm should be taken into consideration when treating tissue such as an ear or nasal cavity with underlying lead shielding.

Compliance with ethical standards

Conflict of interest John Baines declares that he has no conflict of interest. Sylwia Zawlodzka declares that she has no conflict of interest. Tim Markwell declares that he has no conflict of interest. Millicent Chan declares that she has no conflict of interest.

References

1. Klevenhagen SC (1982) The buildup of backscatter in the energy range 1 mm to 8 mm Al HVT. Phys Med Biol 27:1035–1043
2. Lanzon P, Sorell G (1993) The effect of lead underlying water on the backscatter of X-rays of beam qualities 0.5-8 mm Al HVT. Phys Med Biol 38:1137–1144
3. Huq MS, Venkataramanan N, Meli JA (1992) The effect on dose of kilovoltage X-rays backscattered from lead. Int J Radiat Oncol Biol Phys 24:171–175
4. Das IJ, Chopra KL (1995) Backscatter dose perturbation in kilovoltage photon beams at high atomic number interface. Med Phys 22:767–773
5. Hill R, Healy B, Holloway L, Baldock C (2007) An investigation of dose changes for therapeutic kilovoltage X-ray beams with underlying lead shielding. Med Phys 34:3045–3053
6. Healy BJ, Sylvander S, Nitschke KN (2008) Dose reduction from loss of backscatter in superficial X-ray radiation therapy with the Pantak SXT 150 unit. Aust Phys Eng Sci Med 31:49–55
7. Paix D, Taylor K, Holloway A (1983) Backscatter of diagnostic X-rays from metals (communication). Med Phys 10:112–3
8. Yu PKN, Butson MJ (2013) Measurement of effects of nasal and facial shields on delivered dose for superficial X-ray treatments. Phys Med Biol 58:N95–N102
9. Butson JB, Cheung T, Yu PKN (2008) Measurement of dose reductions for superficial a-rays backscattered from bone interfaces Phys. Med Biol 53:N329–N336
10. Baines J, Zawlodzka S, Markwell T, Chan M (2018) Measured and Monte Carlo simulated surface dose reduction for superficial X-rays incident on tissue with underlying air or bone. MedPhys 45:926–933
11. Healy BJ, Gibbs A, Murry RL, Prunster JE, Nitschke KN (2005) Output factor measurements for a kilovoltage X-ray therapy unit. Austr Phys Eng Sci Med 28:115–121
12. Kawrakow I, Rogers DWO (2000) The EGSnrc code system: Monte Carlo simulation of electron and photon transport. NRCC Report PIPRS – 701, Ottawa
13. Rogers DW, Kawrakow J, Seuntjens BR, Walters B, Mainegra-Hing E (2000) NRC user codes for EGSnrc, NRCC Report No. PIRS-702
14. Rogers DWO, Faddegon BA, Ding GX, Ma CM, Wei J, Mackie TR (1995) BEAM: a Monte Carlo code to simulate radiotherapy treatment units. Med Phys 22:503–24
15. Walters B, Kawrakov I, Rogers DWO (2011) DOSXYZnrc users manual NRCC Report PIRS-794revB. NRCC, Ottawa
16. Ma CM, Rogers DWO (2018) BEAMDP users manual. NRCC Report PIRS-0509(C)revA. NRCC, Ottawa
17. Mainegra-Hing E, Kawrakow I (2006) Efficient X-ray tube simulations Med Phys 33:2683–2690
18. Andreo P, Burns DT, Salvat F (2012) On the uncertainties of photon mass energy-absorption coefficients and their ratios for radiation dosimetry. Phys Med Biol 57:2117–2136
19. Chow JCL, Owrangi AM (2012) Surface dose reduction from bone interface in kilovoltage X-ray therapy: a Monte Carlo study of photon spectra. J App Clin Med Phys 13:215–221

20. NIST (2019) X-ray mass attenuation coefficients. http://physics.nist.gov/PhysRefData/XrayMassCoef
21. Eaton JE, Doolan PJ (2013) Review of backscatter measurement in kilovoltage radiotherapy using novel detectors and reduction from lack of underlying scattering material. J Appl Clin Med Phys 14:5–17

Publisher's Note Springer Nature remains neutral with regard to jurisdictional claims in published maps and institutional affiliations.